Scripta Materialia 149 (2018) 79–83

Contents lists available at ScienceDirect

Scripta Materialia

journal homepage: www.elsevier.com/locate/scriptamat

Regular article

Hydrogen trapping in carbon supersaturated α iron and its decohesion effect in martensitic steel

W.T. Geng [a,b,*], Vei Wang [a,c], Jin-Xu Li [b], Nobuyuki Ishikawa [d], Hajime Kimizuka [a], Kaneaki Tsuzaki [e,f], Shigenobu Ogata [a,f,*]

[a] Department of Mechanical Science and Bioengineering, Osaka University, Osaka 560-8531, Japan
[b] University of Science and Technology Beijing, Beijing 100083, China
[c] Department of Applied Physics, Xi'an University of Technology, Xi'an 710054, China
[d] Steel Research Laboratory, JFE Steel Corporation, Kanagawa 210-0855, Japan
[e] Department of Mechanical Engineering, Kyushu University, Fukuoka 819-0395, Japan
[f] Center for Elements Strategy Initiative for Structural Materials, Kyoto University, Kyoto 606-8501, Japan

ARTICLE INFO

Article history:
Received 20 December 2017
Received in revised form 17 February 2018
Accepted 18 February 2018

Keywords:
Hydrogen embrittlement
Dual-phase steel
Martensite
Ferrite
Ab initio calculations

ABSTRACT

Our first-principles calculations demonstrate that hydrogen is more stable in carbon supersaturated martensite than in α iron, due to the carbon-induced tetragonality in martensite lattice. The trapped hydrogen leads to remarkable decohesion between (110) planes both inside the martensite and along the martensite/ferrite interface, with the former being more significant than the latter. This decohesion can explain recent precise observations that in martensite/ferrite dual-phase steels the hydrogen-promoted crack was initiated in the martensite region and that in lath martensite steel it propagated not on lath boundaries but showed quasi-cleavage feature along (110) planes at very high hydrogen concentration.

It is generally accepted that the martensite in steels is more susceptible to hydrogen embrittlement than the ferrite. The atomic-scale mechanism underlying this phenomenon, nevertheless, is not fully understood yet [1]. This is partly due to the structural complexity of martensite lath boundaries, where an elastically and plastically deformed zone [2] contains high density of unpinned dislocations generated by volume expansion in the austenite to martensite transformation [3]. Recently, Koyama et al. [4] observed that in a dual-phase steel the hydrogen-promoted crack was initiated in the martensite region. With content of diffusible hydrogen as high as 10 mass ppm, Shibata et al. [5] found that in a lath martensite steel the hydrogen-promoted crack propagated not on lath boundaries but showed quasi-cleavage feature on (110) planes. Although details of the atomic structure regarding crack initiation are still not clear, these observations point to the significance of hydrogen-induced decohesion inside martensite single crystals in the mechanism of hydrogen embrittlement.

The superior hardness of martensite comes mostly from lattice defects such as solution atoms and high-density of dislocations. Both solution atoms [6] and dislocations [7] can attract hydrogen atoms to some extent, it is therefore expected that hydrogen trapping is more significant in martensite than in ferrite, which obviously plays crucial roles in hydrogen embrittlement of steels [1,8,9]. According to first-principles calculations [6], high concentration solution atoms in steels such as Si, Cr, and Mn repel hydrogen slightly, and C, Ni, and Nb attract hydrogen weakly with binding energies no larger than 0.1 eV/H, remarkably weaker than dislocation hydrogen interactions (about 0.2 eV/H) [6,7]. This comparison suggests that solution atoms might not contribute much to hydrogen trapping in steels. We note, however, in those calculations [6], the concentration of solution atoms is 1.8 at%, but the carbon content in martensite and bainite can be markedly higher than that in early stage of tempering [10] or in carbon-clustered regions [11]. We also note that hydrogen trapping is about 0.34 eV/H in cementite Fe_3C [12]. Thus, it is tempting to ask the question: What is the strength of hydrogen trapping in carbon supersaturated martensite? This issue is relevant to hydrogen embrittlement not only in martensite steels, but also in dual-phase steels where the martensite constitutes a significant part in the ferrite matrix.

We employed $(2 \times 2 \times 2)$, $(3 \times 3 \times 3)$, and $(4 \times 4 \times 4)$ supercells of bcc Fe for the simulation of different carbon concentrations. With one, two, or four carbon atoms in a $(4 \times 4 \times 4)$ supercell (Fig. 1), we can model carbon concentration 0.8 at%, 1.5 at%, and 3.0 at%, respectively. Carbon atoms are put in the octahedral interstitial sites and form a simple cubic, body-centered-cubic, and face-centered-cubic alignment themselves. In this setup, we arranged carbon only in one of the three

* Corresponding author.
E-mail addresses: geng@ustb.edu.cn (W.T. Geng), ogata@me.es.osaka-u.ac.jp (S. Ogata).

https://doi.org/10.1016/j.scriptamat.2018.02.025
1359-6462/

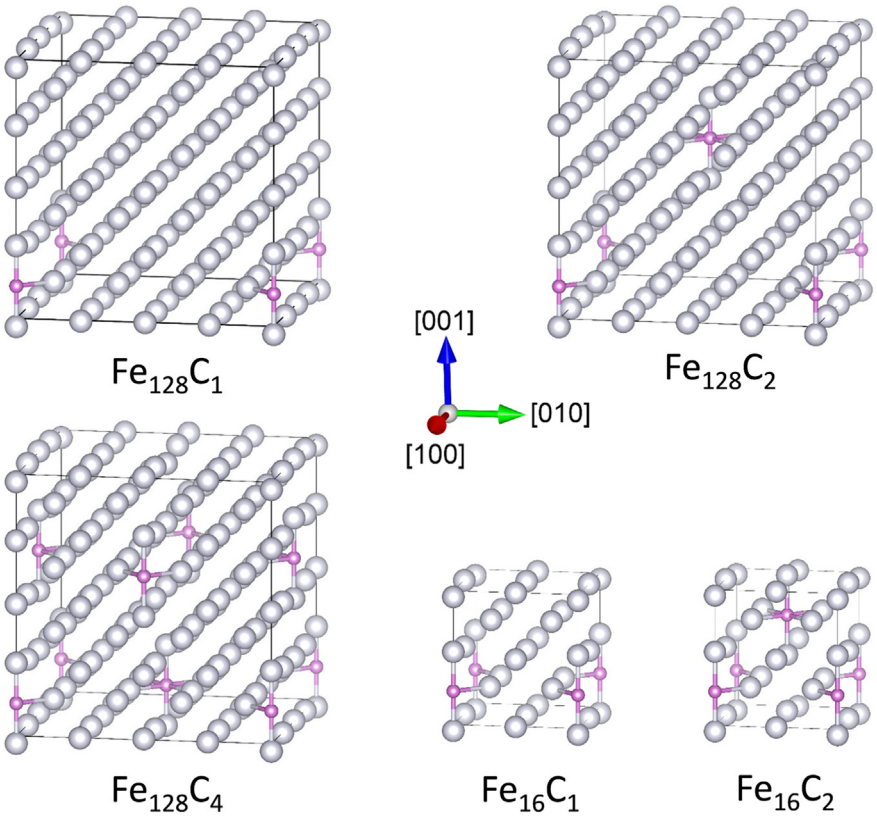

Fig. 1. Supercells used to model different carbon (small spheres) concentration in α iron. Shown here are already optimized structures.

octahedral sub-lattices. This is reasonable in view of the fact that at room temperature, the critical carbon concentration in steel for cubic-to-tetragonal transition through Zener ordering [13] is 0.18 wt% (0.84 at%) [14]. One carbon in a $(3 \times 3 \times 3)$ supercell corresponds to a concentration 1.8 at%, close to the two-in-$(4 \times 4 \times 4)$ case. We performed this calculation for dual purposes. First, we want to compare our result with that from [6] where a $(3 \times 3 \times 3)$ supercell was used. Second, we want to clarify if different carbon alignments, i.e., two-in-$(4 \times 4 \times 4)$ and one-in-$(3 \times 3 \times 3)$ supercell (similar concentration) yield similar tetragonality of the supercell and binding energy with hydrogen. One or two carbon atoms were added into a $(2 \times 2 \times 2)$ supercell (Fig. 1) to model high concentrations 5.9 at% and 11.1 at%. To study hydrogen trapping, we put a hydrogen atom in both tetrahedral and octahedral interstitial sites in the vicinity of carbon in a supercell and determine the most stable position for hydrogen. The trapping (binding) energy for hydrogen ΔE_{trap} is defined as the change in solution energy of hydrogen going from a $(4 \times 4 \times 4)$ supercell of bcc iron (ΔH_s^F) to carbon supersaturated martensite (ΔH_s^M) containing m Fe and n C atoms

$$\Delta E_{trap} = \Delta H_s^F - \Delta H_s^M \tag{1}$$

$$\Delta H_s^F = E(\mathrm{Fe}_{128}H) - E(\mathrm{Fe}_{128}) - \frac{1}{2}E(\mathrm{H}_2) \tag{2}$$

$$\Delta H_s^M = E(\mathrm{Fe}_m\mathrm{C}_n\mathrm{H}) - E(\mathrm{Fe}_m\mathrm{C}_n) - \frac{1}{2}E(\mathrm{H}_2) \tag{3}$$

where E is the total free energy of appropriate supercells and a free standing hydrogen molecule. Similarly, the solution energy of carbon in iron $\Delta H_s(C)$ can be obtained via

$$\Delta H_s(\mathrm{C}) = E(\mathrm{Fe}_m\mathrm{C}_n) - E(\mathrm{Fe}_m) - nE(\mathrm{C}) \tag{4}$$

where E(C) is the total energy of carbon in the state of graphite.

We have performed calculations using density functional theory (DFT) based Vienna Ab initio Simulation Package [15]. The electron-ion interaction was described using projector augmented wave (PAW) method [16]. The exchange correlation between electrons was treated with generalized gradient approximation (GGA) in the Perdew-Burke-Ernzerhof (PBE) form [17]. An energy cutoff of 400 eV was used for the plane wave basis set. The Brillouin-zone integration was performed within the Monkhorst-Pack scheme [18] using k meshes of $(6 \times 6 \times 6)$, $(4 \times 4 \times 4)$, and $(3 \times 3 \times 3)$ for $(2 \times 2 \times 2)$, $(3 \times 3 \times 3)$, and $(4 \times 4 \times 4)$ supercells, and a k meshes of $(1 \times 4 \times 3)$ for the $(6\sqrt{2} \times 2 \times 2\sqrt{2})$ supercells used to compute the cleavage energy. The energy relaxation for each strain step was continued until the forces on all the atoms were converged to less than 1×10^{-2} eV Å^{-1}. Both shape and volume of the supercell of iron, aside from the internal coordinates, were optimized upon introducing carbon atoms. When adding hydrogen into the carbon supersaturated iron, however, we have optimized only the internal coordinates for all atoms in the supercell because the hydrogen atom is much smaller than iron. In all calculations, spin-polarization was allowed to take into account of the magnetic nature of bcc Fe. Moreover, zero-point vibration of H atoms was also taken into account.

The calculated solution energy of carbon in α-Fe at various concentrations is listed in Table 1. The value for 0.8 at%, 0.62 eV/C, is 0.12 eV smaller than previous DFT [19]. We note that the energy cut-off used in [19] was 350 eV, which may not be large enough. The value for 5.9 at%, 0.59 eV/C, is slightly smaller than the previous DFT calculation using all-electron method [20], 0.65 eV/C. We need to point out that the small variation in the solution energy of carbon in the concentration

Table 1
Solution energy ΔH_s(C) (in eV/C) of interstitial carbon (in at%) in α-Fe. The concentration is in atomic percentage. Positive values indicate endothermic processes.

	0.8%	1.5%	1.8%	3.0%	5.9%	11.1%
$\Delta H_s(C)$	0.62	0.59	0.62	0.52	0.59	0.41